Near-Infrared Emitting Fluorophore-Doped Calcium Phosphate Nanoparticles for *In Vivo* Imaging of Human Breast Cancer

Erhan İ. Altınoğlu,[†] Timothy J. Russin,[‡] James M. Kaiser,[§] Brian M. Barth,[§] Peter C. Eklund,[†,‡] Mark Kester,[§] and James H. Adair[†,*]

[†]Department of Materials Science and Engineering, [‡]Department of Physics, Pennsylvania State University, University Park, Pennsylvania 16802, and [§]Department of Pharmacology, College of Medicine, Pennsylvania State University, Hershey, Pennsylvania 17033

ABSTRACT Early detection is a crucial element for the timely diagnosis and successful treatment of all human cancers but is limited by the sensitivity of current imaging methodologies. We have synthesized and studied bioresorbable calcium phosphate nanoparticles (CPNPs) in which molecules of the near-infrared (NIR) emitting fluorophore, indocyanine green (ICG), are embedded. The ICG-CPNPs demonstrate exceptional colloidal and optical characteristics. Suspensions consisting of 16 nm average diameter particles are colloidally stable in physiological solutions (phosphate buffered 0.15 M saline (PBS), pH 7.4) with carboxylate or polyethylene glycol (PEG) surface functionality. ICG-doped CPNPs exhibit significantly greater intensity at the maximum emission wavelength relative to the free constituent fluorophore, consistent with the multiple molecules encapsulated per particle. The quantum efficiency per molecule of the ICG-CPNPs is 200% greater at 0.049 ± 0.003 over the free fluorophore in PBS. Photostability based on fluorescence half-life of encapsulated ICG in PBS is 500% longer under typical clinical imaging conditions relative to the free dye. PEGylated ICG-CPNPs accumulate in solid, 5 mm diameter xenograft breast adenocarcinoma tumors *via* enhanced retention and permeability (EPR) within 24 h after systemic tail vein injection in a nude mouse model. *Ex situ* tissue imaging further verifies the facility of the ICG-CPNPs for deep-tissue imaging with NIR signals detectable from depths up to 3 cm in porcine muscle tissue. Our *ex vivo* and *in vivo* experiments verify the promise of the NIR CPNPs for diagnostic imaging in the early detection of solid tumors.

KEYWORDS: calcium phosphate · indocyanine green · nanoparticles · encapsulation · near-infrared · bioimaging · EPR effect · photophysics · whole animal imaging

The advantages associated with early detection of disease[1] have initiated much interest in exogenous contrast agents as a means of optically imaging markers unique to specific cell types at the onset of a disease, such as breast cancer, far in advance of changes on the gross anatomic level.[2−4] Fluoroprobes, for example, are being developed to achieve this selective imaging sensitivity,[5] particularly those that work in the near-infrared (NIR, 700−900 nm) spectrum, a wavelength region of low absorptivity by tissue chromophores.[6] This permits fluorescence signals relatively free of intrinsic background interference with detectable signal intensities through several centimeters of tissue.[3,7]

Indocyanine green (ICG) is a NIR contrast agent which has been widely investigated for use in deep-tissue imaging and is the only NIR organic dye approved by the U.S. Food and Drug Administration (FDA) for human use.[8] ICG is an amphiphilic carbocyanine dye that exhibits absorption and emission maxima around 780 and 820 nm, respectively.[9−11] Due to its low toxicity (LD_{50} of 50−80 mg/kg for animal subjects[12]), ICG is used clinically as a contrast agent for optical imaging in angiography[13] and guiding biopsies,[14] as well as for evaluating blood flow[15,16] and hepatic function.[17,18] It is one of the least toxic contrast agents administered to humans,[19] with the only known adverse reaction being rare anaphylaxis.[20]

However, as with many organic dye molecules, ICG has a low fluorescence quantum yield due to internal conversion[21,22] and is prone to photobleaching, solvatochromic effects, and nonspecific quenching, all of which limit its utility in sensitive and prolonged *in vivo* imaging applications.[7,10,21,23,24] Numerous efforts have reported the optical instability of ICG in physiologically relevant solutions such as water,[11,25,26] salt solutions,[11,27] plasma,[11,26,27] and blood.[26,28−30] In such environments, oxidation and dimerization degrade the original molecule, resulting in decreased absorption, reduced fluorescence, and variability in the maximum absorption wavelength.[31,32] Furthermore, ICG often binds to proteins[33] leading to rapid agglomeration and subsequent elimination

*Address correspondence to jha3@psu.edu.

Received for review July 16, 2008 and accepted August 29, 2008.

Published online September 19, 2008.
10.1021/nn800448r CCC: $40.75

from the body with a plasma half-life from 2 to 4 min.[25,29]

Sensitive, real-time *in vivo* monitoring schemes require that a fluoroprobe retain its state of dispersion in physiological environments, sustain a strong, prolonged signal intensity, accumulate in targeted regions of interest, and passively resorb into the body upon completion of function.[5] One of the significant advantages nanotechnology has brought to bioimaging is the capacity to improve various fluoroprobe molecules for *in vivo* applications.[5,34] An assortment of nanoparticulate systems have been developed to encapsulate fluorescent molecules for bioimaging applications; the reader is directed elsewhere for comprehensive reviews of these various colloidal carriers.[24,35] A primary significance of these particulate modifications is the extension of circulation half-life and *in vivo* stability relative to the free constituent fluoroprobe molecules.[10,36] Several studies also report the amplified optical emission for a single particle containing multiple fluorophores relative to a single fluorophore molecule.[37−40] Perhaps the most promising attribute of fluorophore-doped particles is the improved photostability of the encapsulate by both the inhibition of unfavorable conformational reorganization[22] and reduced interactions with solvent molecules, which avoid dynamic processes that result in nonradiative energy losses.[41]

Polymer-based carriers are one of the most common types of particulate systems employed for *in vivo* applications[42] due to high biocompatibility and the facility with which resorbability is achieved.[43] Recent years have witnessed numerous polymeric modalities to address the intrinsic issues of ICG degradation and rapid blood clearance.[10,44−46] However, these efforts fall short in improving the optical performance for deep-tissue imaging schemes.[10] Saxena *et al.*[47] first improved aqueous and thermal stabilities by encapsulating ICG within ~350 nm poly(lactic-*co*-glycolic acid) (PLGA) particles, but these carriers suffered significant leakage with 78% ICG loss within 8 h in physiological conditions. Subsequently, a silica−polymer composite microcapsule was developed to improve encapsulated ICG retention (17% ICG leakage after 8 h at 37 °C),[10] but the addition of the nanoparticulate shell increased the particle size to 1 μm. However, the polymer network gives the encapsulated molecules little protection from dimerization or photoisomerization, as evidenced by the red shift in the peak absorbance wavelength[10,46,48] and a significant decrease in peak fluorescence intensity.[47] Recent work has improved embedded ICG molecules' performance in organically modified silicates,[49] but the 100 nm silicate carriers lie on the upper limit of the preferred size range for *in vivo* applications.[50,51]

Calcium phosphate (CP) is a primary biomineral that is ubiquitously present in the body[52] and whose functions have long been exploited in biocompatible[53−55] bone substitutes and biodegradable adjuvants.[56] Several issues arise when employing exogenous agents for *in vivo* use, particularly the cytotoxicity to organelles and induction of apoptosis,[57] as well as the deposition and clearance from the body.[34] Recent reports have attributed such toxicity to the intracellular degradation of the endocytosed particles into their constituent components.[58−61] For instance, a concern for semiconductor quantum dot (QD) use lies in the presence of heavy metals such as CdSe, which are reportedly toxic to cells even at low concentrations (10 μM/mL).[62] Unlike most of its counterparts, the constituent ions of biodegradable CP particles (Ca^{2+} and PO_4^{3-}) are ubiquitously present at millimolar concentrations within the bloodstream.[63] Due to this established compatibility and low immune response,[56,64] many recent efforts[65−70] have reported CP preparation as particles for nontoxic and efficient transport of bioactive agents.

The objective of this work is to report a novel carrier system for sensitive deep-tissue NIR imaging using sub-50 nm, biocompatible CP nanoparticles (CPNPs), colloidally stable in physiological solutions, which exploit the matrix-shielding effect and thereby impart improved fluorescence properties to the encapsulated ICG suitable for sensitive, early state diagnostic imaging.

RESULTS AND DISCUSSION

Synthesis and Characterization of NIR Dye-Doped Calcium Phosphate Nanoparticles (CPNPs). Spherical CPNPs doped with ICG were synthesized using aqueous coprecipitation of calcium chloride and disodium hydrogen phosphate in the presence of disodium silicate within water-in-oil microemulsions as described in Materials and Methods. ICG doping was accomplished through the designed addition of the fluorophore into the microemulsion during precipitation. Particle stability was fostered through electrosteric repulsion *via* citrate surface functionalization.[71] Particle suspensions were then laundered *via* a van der Waals high performance liquid chromatography (vdW-HPLC) protocol adopted from our previous work to remove residual synthetic components and concentrate the particles in a 7:3 by volume ethanol:water mixture.[72] Colloidal characterization included the size distribution, morphology, and colloidal state of dispersion of the collected nanoparticle suspensions using transmission electron microscopy (TEM).

Figure 1A is a TEM micrograph of the ICG-doped CPNPs. The figure underscores the well dispersed state of the suspension, with the magnified inset (Figure 1B) illustrating the representative particle size and spherical morphology. The figure also includes a schematic representation of the CPNP architecture (Figure 1C), illustrating the encapsulated imaging agent internalized within the CP matrix and fully covered with surface functional groups. Atomic force microscopy data (not shown) verifies the spherical morphology of the particles. The log-normal mean particle diameter and standard deviation is 16 nm and $\sigma_z = 0.23$, respectively ($n = 932$), based on

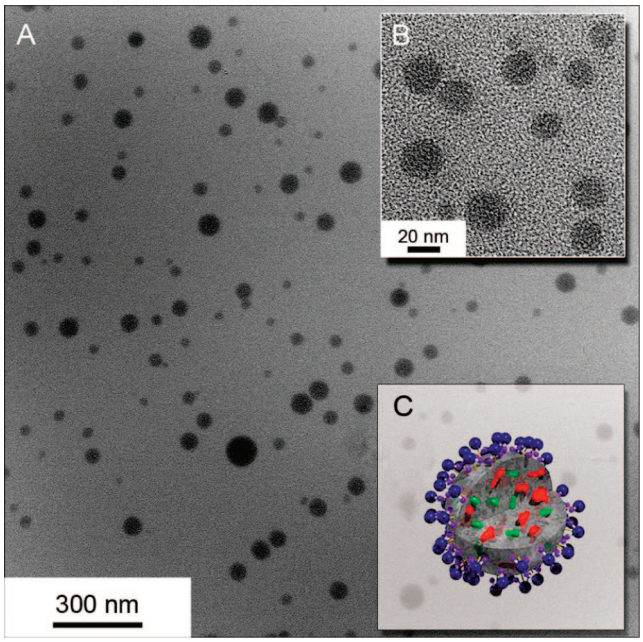

Figure 1. (A) TEM micrograph of a dye-encapsulating ICG-CPNP dispersion with (B) magnified inset showing the particles in detail. The log-normal mean and standard deviation of the particle number distribution is 16 nm ($n = 932$) with a σ_z equal to 0.23, respectively. (C) Schematic representation of CPNP architecture showing encapsulated imaging agent (green) and any alternate payload (red) with full surface functionalization (blue).

TEM image analysis. This size range falls within the accepted window for the most efficient cellular uptake (≤50 nm) and closely matches the optimal size of 25 nm for receptor-mediated endocytosis.[51] The electrophoretic mobility, used to verify surface charge on the ICG-doped particles, cannot be measured with the present instrumentation due to the absorption of the 636 nm laser by the embedded ICG fluorophore. Surface charge has, however, been determined using light scattering particle electrophoretic mobility for a variety of functional groups on CPNP surfaces that encapsulate alternate fluorophores; citrate functionalization gives a negative ζ potential of −30 mV (data not shown).

Optical Properties of NIR Dye-Doped CPNPs. Emission Enhancement. The fluorescence spectrum of the dye-doped CPNPs was compared to that of the corresponding free ICG dye under identical optical conditions (785 nm excitation). Figure 2 shows that the shape of both the absorption and emission curves are similar for free ICG and the doped nanoparticles in aqueous solution. This indicates that the encapsulation of the fluorophore within the rigid CP matrix, unlike polymeric encapsulation, retains the monomeric state of the encapsulated ICG without deleterious structural or chemical alterations that adversely affect absorption and emission of the dye. These undesirable phenomena result in peak transformations or spectral shifts, respectively, which are not observed for the embedded ICG spectra.

The fluorescence emission intensity of one dye-doped CPNP is approximately 10^3 times that of one ICG dye molecule as shown in Figure 2. The enhanced brightness is similar to reports by Zhao *et al.* on fluorescent silica nanoparticles.[37] However, this enhanced brightness is at least partly due to the nanoparticle architecture, with multiple dye molecules encapsulated in a single particle. Thus, brightness or intensity does not provide evidence that the encapsulation provides intrinsically different fluorescence performance than the free molecules. Nonetheless, the encapsulated ICG is uniformly distributed and not self-aggregated in the calcium phosphate matrix based on the elevated intensity for the overall encapsulated 10^{-5} M ICG. In contrast, self-aggregation and loss of emission intensity of free ICG occurs in aqueous solution at 7×10^{-6} M at pH 7 (data not shown). To assess whether the elevated brightness is intrinsic to the encapsulated ICG, the quantum efficiency per molecule is presented and discussed.

Quantum Efficiency. The fraction of photons absorbed by a molecule that are emitted *via* a fluorescence photon is quantum efficiency (QE). Thus, QE is the ratio of the number of excited-state fluorophores that relax *via* a fluorescent transition to the total number of excited-state relaxations that occur (including fluorescence, as well as other nonradiative mechanisms such as internal conversion, vibrational relaxation, intersystem crossing, photoisomerization, or combinations thereof).[22,23] The QE provides a metric for the potential of a fluoroprobe in imaging schemes; for sensitive or long-term imaging

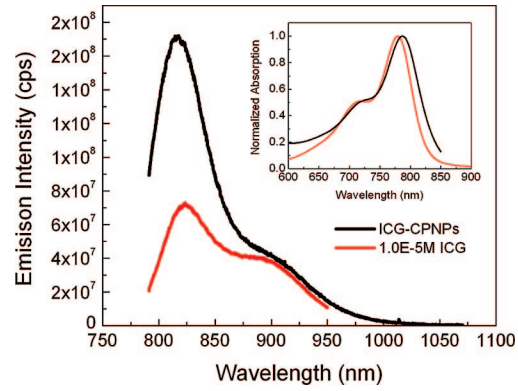

Figure 2. Absorption (inset) and fluorescence spectra of free ICG (red) and ICG-CPNPs (black) in aqueous solution. The CPNP suspension (10^{13} particles/mL) had an apparent fluorophore content of roughly 10^{-5} M based on absorption standards; a matching concentration of free dye was used for the comparison. The shape and position of both the absorption and emission spectra are similar, indicating the absence of either chemical modification or dimerization upon encapsulating the dye in the calcium phosphate matrix. Emission from the ICG-CPNPs is significantly brighter than the matching free dye solution, which suffers from quenching interactions due, in part, to free dye self-aggregation.

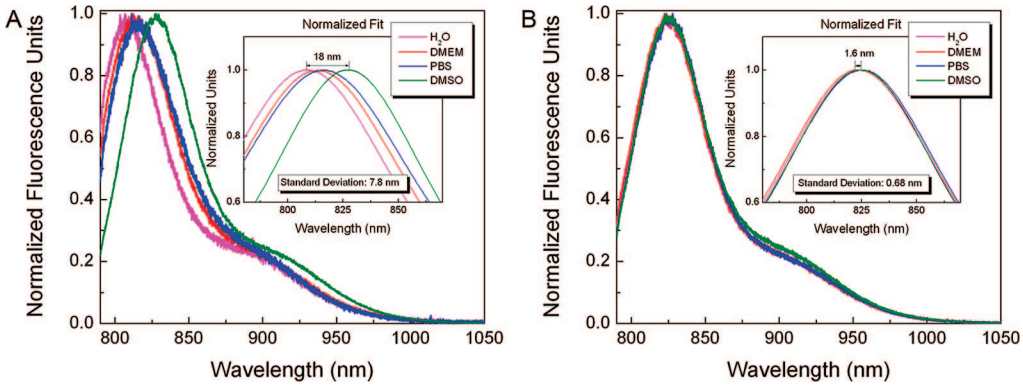

Figure 3. Comparative spectral effect of four biorelevant solvents on the emission response of (A) free ICG dye and (B) dye-doped ICG-CPNPs. The normalized peaks spread across 18 nm for the free fluorophore (standard deviation of 7.8 nm), while encapsulation in CPNPs has an order of magnitude smaller 1.6 nm spread (0.68 nm standard deviation). These data confirm the largely impermeable nature of the CP matrix to the surrounding environment, shielding the encapsulated dye from solvent interaction.

applications, the fluorescence of the ideal fluoroprobe dominates over competing energy loss pathways, resulting in efficient conversion of absorbed photons to emitted fluorescence signal. Despite widespread use in medical imaging, the QE for the ICG monomer in aqueous solution is only 0.027 ± 0.005[21] with values as low as 0.01 reported.[22] Loss for ICG is primarily due to internal conversion[21] since intersystem crossing mechanisms amount to a minimal rate of triplet formation.[73] The relative QE of dye-encapsulating ICG-CPNPs in phosphate buffered 0.15 M saline (PBS) was compared to that of free ICG molecules in the same environment, measured against the near-infrared laser dye hexamethylindotricarbocyanine (HITC) as a reference of known quantum yield (0.28).[74] The measured free ICG QE in high ionic strength, pH 7.4 PBS (0.028 ± 0.001), is likely a result of significant dimerization, consistent with similar reports on aggregate formation.[21] Physically bound ground-state dimers and oligomers act as quenching centers of fluorescence due to the energy transfer between excited and nonexcited states.[75] Thus, the reduced QE in PBS of the free dye indicates an increase in nonradiative decay rates among aggregates.

However, the QE of the doped CPNPs in PBS is 2-fold greater (0.049 ± 0.003), with the CP matrix preventing environmental effects and dimerization, reducing the occurrence of nonradiative energy transfers. Furthermore, this result presents an objective explanation for the increased brightness from the ICG-CPNPs relative to the free fluorophore. Thus, CPNPs doped with ICG exhibit intrinsically greater brightness and enhanced QE relative to the free dye for *in vivo* and *in vitro* applications.

Solvent Protection. The chemical stability of the encapsulated fluorophore was experimentally verified by analyzing fluorescence spectra as a function of solvent environment. The effect of four biorelevant solvents (water, Dulbecco's modified Eagle's medium (DMEM), ethylene glycol, and dimethylsulfoxide (DMSO)) on the free ICG dye is shown in Figure 3A, with shifts in the normalized emission spectra dependent on the solvent environment. The maximum emission wavelengths have a standard deviation of 7.8 nm over an 18 nm spread. These peak values shift toward longer wavelengths due to a combination of general solvent influences and specific solvent effects, such as molecule−molecule interactions and hydrogen bonding.[23]

In contrast, the emission spectra for the encapsulated dye in CPNPs are stable regardless of solvent environment. Figure 3B (peak standard deviation of 0.68 nm, 1.6 nm spread) highlights the impermeable nature of the CP matrix to the solvent environment, which shields the dopant fluorophore from solvent interactions and prevents oxidative and solvent-induced alterations.

Photostability. Photobleaching is often a consequence of chemical and solvent interactions and is typically credited to a reaction between the fluorophore molecule and dissolved oxygen.[22] The encapsulated ICG molecules are protected from environmental oxygen in the CPNP fluoroprobe system, as evidenced by a notable increase in the half-life of the encapsulated dye *versus* the free dye when subjected to continuous illumination (Figure 4). The CPNP has a matrix shielding effect, which permits prolonged periods of excitation without significant degradation in emission intensity. Free ICG dye and doped CPNPs were excited under continuous illumination from a diode laser (785 nm; 450

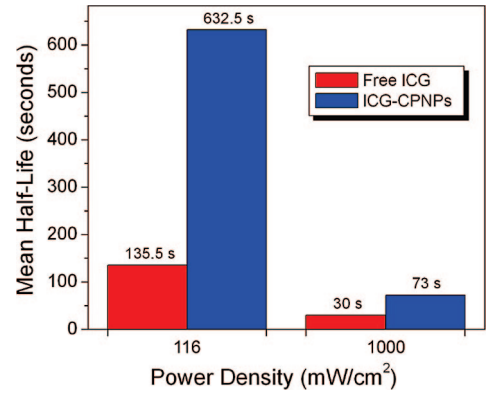

Figure 4. Fluorescent half-life for a free ICG fluorophore (red) and ICG-CPNP (blue) suspension of matching absorption (10^{-6} M) in PBS under 785 nm excitation at two power densities. Encapsulation provides an average of 470% increase in half-life at an excitation power commonly used in clinical settings (~100 mW/cm^2) and a 240% increase under extremely high laser power density (1000 mW/cm^2).

mW/cm^2) at comparable concentrations in PBS (pH 7.4) to mimic the physiological environment. Data in Figure 4 show that CPNP encapsulation gives approximately a 500% increase in emission half-life at laser power slightly higher than typical clinical NIR imaging applications (5 to 50 mW/cm^2)[76] and even provides a 240% increase under extremely high laser power conditions (1000 mW/cm^2).

***In Vivo* Pharmacokinetic Distribution and Tumor Localization in Nude Mice.** A NIR whole animal imaging approach was used to investigate the *in vivo* pharmacokinetic distribution of ICG-CPNPs in nude mice. Figure 5 gives the fluorescence signal and intensity distribution as a function of time for ICG-CPNPs delivered systemically *via* tail vein injections. Two different surface functionalities of CPNPs were evaluated, as-synthesized carboxylate surface termination (not shown) and particles surface functionalized with polyethylene glycol (PEG) (series iii). The *in vivo* behavior of the ICG-CPNP samples was compared to two controls: a sample of carboxylated ghost CPNPs without a fluorescent encapsulate (series i) and free ICG of equivalent absorption (series ii). The fluorescence signals from the ICG-encapsulating CPNPs are significantly prolonged *in vivo* compared to the free fluorophore; no detectable signal was recorded from the free ICG at 24 h after injection (Figure 5B). In contrast, the ICG-CPNPs retained significant fluorescence signals even after 4 days (Figure 5C). The relatively short *in vivo* fluorescence of the free dye is attributed to fluorescence quenching of free ICG in physiological environments[11,25−27,29,30] with rapid aggregation and clearance from the body.[25,29] The lipophilic character of ICG means it is taken up exclusively by hepatic parenchymal cells where it is then secreted into the bile.[25] This clearance pathway is consistent with our observations of initial hepatic localization and eventual total clearance through the biliary tree with minimal acute renal involvement. Figure 5D illustrates excised organs 10 min after systemic injection of PEGylated ICG-CPNPs. Additional dissections at longer time points affirmed this hepatobiliary clearance route with detectable signals along the gastrointestinal route (images not shown). Negligible movement of fluorescence across the blood−brain barrier was observed. The hepatobiliary clearance mechanism offers yet another unique advantage of the calcium phosphate nanoparticles. The lack of long-term accumulation within the liver, as well as minor renal imaging, suggests minimal potential for hepatic or renal toxicology. Moreover, the lack of brain imaging suggests that barriers, such as the blood−brain barrier, are relatively impermeable to the carboxylate- or PEG-CPNPs.

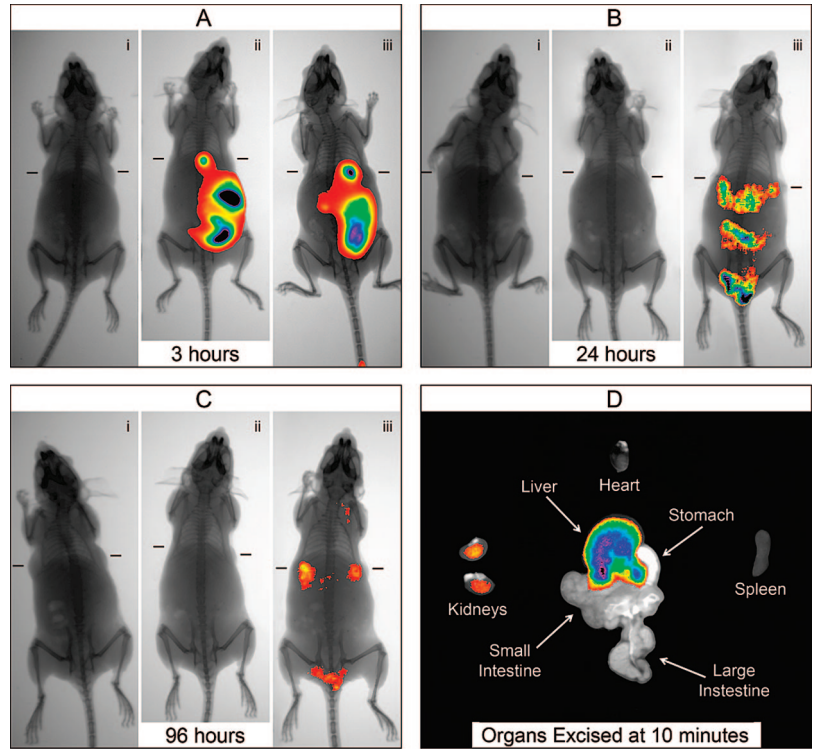

Figure 5. NIR transillumination images (Ex. 755 nm, Em. 830 nm) taken at various times track fluorescence signals and pharmacokinetic distributions for the ICG-CPNPs and controls delivered systemically *via* tail vein injections in nude mice implanted with subcutaneous human breast adenocarcinoma tumors. Hash marks next to each mouse indicate the position of the 5 mm tumors. Two control samples, (i) carboxylate-terminated CPNPs without ICG encapsulant and (ii) free ICG, match the particle concentration and fluorophore content (10^{13} particles/mL and 10^{-5} M, respectively) of a (iii) PEGylated ICG-CPNP sample. (Bii) No fluorescence signal is detected from the free ICG at 24 h postinjection, while the PEG-ICG-CPNP sample (Ciii) retains significant signal even after 96 h. (Biii) Fluorescence signal is unmistakably localized in tumors 24 h after administration with PEGylated ICG-CPNPs. The excised organs in panel (D) illustrate the biliary clearance route 10 min postinjection of PEG-ICG-CPNPs. Fluorescence signal is not seen from the stomach or spleen with minimal renal involvement.

Consistent with the *ex situ* analyses presented above, the matrix shielding effect provided by the CPNPs retards deleterious emission loss in circulation, permitting greater fluorescence emission and extended circulation times for the encapsulated dye. This effect is consistent with a similar report of a polymeric *in vivo* delivery scheme.[77] A comparison of signal intensity localized within the liver and along the hepato-gastrointestinal tract at the 3 h time point (Figure 5A) shows a lower concentration of ICG-CPNPs undergoing hepatic uptake and bile secretion relative to the free dye control, further confirming that a greater concentration of ICG-CPNP remains in circulation than free dye.

Our preliminary *in vivo* imaging study also underscores an additional advantage from the prolonged circulation afforded by the CPNPs. The longer retention times permit the particles to passively collect in the breast cancer tumors. Macromolecules and small particles with sufficient circulation times will eventually extravasate and accumulate in solid tumors[78] *via* a pas-

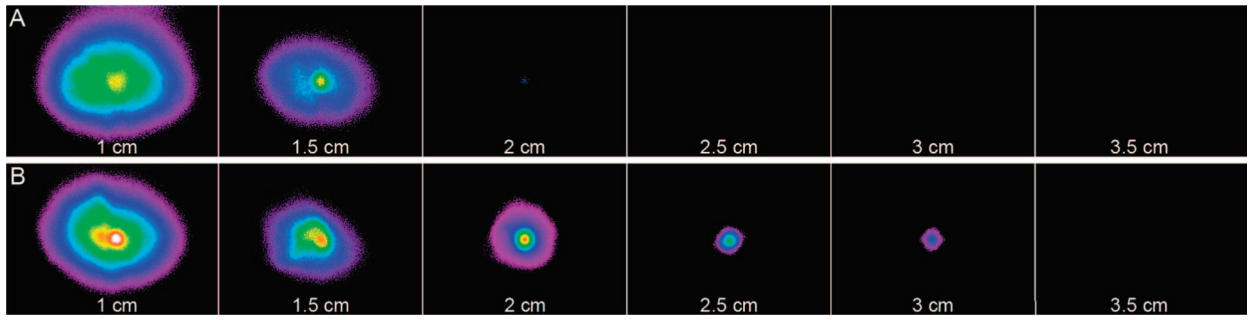

Figure 6. Fluorescence signal intensity as a function of depth in dense porcine muscle tissue of (A) free ICG and (B) ICG-CPNPs of comparable absorbance (10^{-4} M). A 15 mW laser diode (785 nm) and modified consumer-grade digital camera fitted with an 850 nm bandpass filter set were used for excitation and detection, respectively. Detectable penetration depths are extended to 3 cm with CPNP encapsulation compared to the free fluorophore (2 cm) under identical imaging parameters (F3.5, 7 s exposure).

sive mechanism referred to as the enhanced permeability and retention (EPR) effect.[79,80] EPR has been attributed to the leaky nature of tumor blood vessels, which contain large interendothelial junctions, an imperfect basement membrane, an inefficient lymphatic system, and large numbers of transendothelial channels.[81] Figure 5B shows that the PEGylated ICG-CPNPs accumulate in the two subcutaneous tumors within 24 h after injection, which is consistent with previously reported improvements in circulation half-lives for PEGylated quantum dots[82] and EPR tumor accumulation periods for PEGylated gold nanoshell particles.[83] The carboxylate-functionalized CPNPs also showed distinct tumor localization (data not shown) but at significantly lower signal intensities than the PEGylated particles. The PEGylation provides physiological dispersion and inhibits protein absorption, providing maximum retention in the circulatory system to exploit the EPR effect. The *in vivo* imaging studies were replicated in five separate groups of mice.

These initial data provide strong evidence that CPNP encapsulation of ICG is sufficient for *in vivo* shielding to provide prolonged fluorescence emission over 4 days post systemic injection. Furthermore, our preliminary animal imaging shows that PEGylated CPNPs have sustained *in vivo* circulation that provides the tumor retention that is crucial for diagnostic imaging applications.

Tissue Imaging. Fluorescence signals through *ex situ* tissue were imaged under nonoptimal conditions to demonstrate the deep-tissue imaging capacity of the ICG-CPNPs. Figure 6 presents the pseudocolored NIR intensities as a function of depth into porcine muscle tissue of free ICG and a sample of ICG-CPNPs of comparable absorbance (10^{-4} M), both of which were front-face illuminated with excitation at 785 nm and recorded under identical imaging conditions using an 850 nm bandpass filter set on a NIR-modified commercial CCD camera. Detectable penetration and emission depths are seen with ICG-CPNPs to 3 cm compared to the weakly fluorescent free fluorophore at only 2 cm. The signal intensity from the ICG-CPNPs also highlights the optically transparent nature of the CPNP carriers to the emission wavelength, an essential criterion for sensitive tissue imaging applications. The denser muscle tissue has a total optical attenuation coefficient of $\mu_t = 541$ cm^{-1} at 515 nm wavelength.[84] Tissue of lower optical density, such as breast and epithelial tissues with $\mu_t = 189$ and 243 cm^{-1} at 633 nm, respectively,[84] permit even greater detectable signal depths. Furthermore, our use of a commercial laser diode for excitation and an inexpensive commercial CCD camera modified for NIR imaging emphasizes the potential for ICG-CPNP imaging applications where portability and ease of operation, such as in the surgical operating theater, are critical requirements.

CONCLUSIONS

The optical, biophysical, and chemical properties of the PEGylated ICG-CPNPs are well suited for early stage *in vivo* tumor imaging. Bioresorbable calcium phosphate was used to encapsulate the near-infrared emitting fluorophore indocyanine green (ICG) as a new nanoparticulate fluoroprobe for sensitive diagnostic imaging. Suspensions of ICG-CPNPs consist of 16 nm mean diameter particles with a carboxylate or PEG surface termination that provides electrosteric dispersion in physiological conditions. The nanoparticle-based system readily satisfies the critical size for efficient *in vivo* cellular uptake (<50 nm) and the colloidal criteria of robust dispersion in physiological conditions for successful use as an exogenous probe in long-term bioimaging applications. Furthermore, the ICG-encapsulating CPNPs have significantly better optical properties compared to the free fluorophore. The maximum fluorescence peak is not affected by encapsulation and exhibits higher emission intensity relative to the free fluorophore at elevated concentrations. The CP matrix is impermeable to the surrounding solvent, effectively sequestering the ICG from environmental influence. The dye-doped CPNPs have a 4.7-fold longer fluorescent half-life at clinical imaging excitation power ranges and a 2-fold increase in quantum efficiency in PBS (0.049 ± 0.003). These properties provide increased brightness and prolonged signal intensity vital for sensitive diagnostic applications. Furthermore, the PEGylated CPNP encapsulation also provides prolonged circulation times *in vivo* with passive tumor accumulation

of the nanoparticles seen by 24 h after systemic administration that persists more than 96 h postinjection. Finally, preliminary tissue imaging verified the capacity of these NIR CPNPs for deep-tissue imaging applications, revealing extended signal detection depths of at least 3 cm compared to the free fluorophore. Our current studies are evaluating longer term effects of more specifically targeted ICG-CPNPs for both *in vivo* imaging and photodynamic therapy of cancer. Combined with the established biocompatibility and facile resorbability of calcium phosphates, the physical and optical properties of ICG-encapsulating CPNPs represent an attractive new fluoroprobe for sensitive diagnostic imaging applications.

MATERIALS AND METHODS

Materials. All chemicals used in this work were purchased as described: calcium chloride dehydrate (99+%, ACS Reagent), sodium hydrogen phosphate (99+%, ACS Reagent), disodium citrate dehydrate (99+%, ACS Reagent), sodium silicate solution (~14% NaOH, ~27% SiO_2), ethyl-*N*-(3-dimethylaminopropyl)-*N*′-hydrochloride carbodiimide (Fluka BioChemika ≥99.0% AT), dimethylsulfoxide (≥99.9%, ACS Reagent), Dulbecco's Modified Eagle's Medium, and ethylene glycol (99.8%, Anhydrous) from Sigma Aldrich (St Louis, MO); indocyanine green from TCI America (Portland, OR); cyclohexane (99.9+%, A.C.S Reagent), and methanol (99.9+%, OmniSolv spectroscopic grade) from VWR International (West Chester, PA); Igepal CO-520 from Rhodia Inc. (Cranbury, NJ); ethyl alcohol (200-proof, Absolute, ACS/USP grade) from Pharmco-AAPER (Brookfield, CT); methoxypolyethylene glycol amine (mPEG-amine, MW 20 kDa) from JenKem Technology USA (Allen, TX); 1,1′,3,3,3′,3′-hexamethylindotricarbocyanine iodide from Exciton (Dayton, OH); fetal bovine serum (35-010-CV, Regular) from Mediatech, Inc. (Manassas, VA); trypsin (soybean) from Invitrogen (Carlsbad, CA).

All HLPC solutions were prepared with CO_2-free deionized water (pH 7). Water was deionized in our laboratory using a Millipore Milli-Q purification system (Billerica, MA), passed through a 200 nm filter, and boiled while flushing with argon to remove CO_2. All pH measurements were performed using a Sentron ISFET pH probe (Argus IP 65 ISFET; Sentron Inc., The Netherlands) calibrated against aqueous standards.

Synthesis and Characterization of NIR Dye-Doped CPNPs. Dye-doped calcium phosphate nanoparticles (CPNPs) were synthesized employing a double reverse microemulsion approach. The two reverse microemulsions were formed by a cyclohexane/nonylphenoxyl (glycolether) (Igepal CO-520)/water system; 650 μL of 10^{-2} M $CaCl_2$ was added to 14 mL of a 29 vol % solution of Igepal CO-520 in cyclohexane (microemulsion A), while 65 μL each of 6×10^{-3} M disodium phosphate and 8.3×10^{-3} M disodium silicate was added to a separate 14 mL of a 29 vol % Igepal CO-520/cyclohexane mixture (microemulsion B). The dopant fluorophore (520 μL of 10^{-2} M ICG) was added to microemulsion B based on charge considerations to preclude coprecipitation inhibition that can occur once calcium binds to the sulfonate groups present on the fluorophore molecule. All solutions were in CO_2-free deionized water (pH 7) unless otherwise noted. The microemulsions were equilibrated under constant stirring for 1 h before being combined to form a microemulsion mixture (microemulsion C) which served as a microreactor for the coprecipitation of the ICG-doped CPNPs. Microemulsion C was stirred for 2 min before the dispersant, 225 μL of 10^{-3} M sodium citrate, was added and stirred for an additional 15 min. Finally, the micelles were disrupted with 50 mL of pH 7 ethanol before laundering *via* a van der Waals high performance liquid chromatography (vdW-HPLC) procedure, whereby control of electrostatic charge during different stages of the laundering procedure washes and separates the concentrated particle suspension from the synthesis precursors.

The particles were washed by first loading the sample solution onto a chromatography column containing silica microspheres (Stellar phases Inc., Langhorne, PA, ~20 μm diameter, 60 Å pores). During this loading, the CPNPs adhered to the silica media due to the negligible surface charge present in the low dielectric solution of the postdisrupted sample volume, which was approximately 25 v/o cyclohexane in ethanol. The system was then flushed with pH-adjusted ethanol (pH 7) and monitored at the characteristic absorption wavelength of ICG (785 nm) using a UV−vis absorption detector (Shimadzu SPD-6A; Shimadzu Scientific, Kyoto, Japan). The ethanol mobile phase swept the synthesis precursors and any unencapsulated dye through the column, while the relatively large van der Waals attraction between the CPNPs and column media caused retention of the particles within the column. This washing step was concluded only when the detector reached the preset baseline, indicating the removal of residual free dye. The CPNPs, which remained bound on the column, were then eluted with a 7:3 ethanol:water solution, which provided enough charge for electrostatic repulsion to dominate the CPNP−silica media interaction energies, allowing the particles to traverse down the column for collection. The first major peak, corresponding to the elution of the doped particles, was collected. The mobile phase ethanol was adjusted to pH 7 with small additions of 1 M aqueous KOH. The eluent was prepared with CO_2-free deionized water and also adjusted to pH 7 with 1 M KOH.

The size, morphology, and state of dispersion of the nanoparticles were characterized using a Philips 420 TEM on carbon support film on a 300-mesh copper specimen grid (#CF300CU; Electron Microscopy Sciences, Hatfield, PA). Each TEM specimen was prepared by dropping as-prepared CPNPs in 70:30 ethanol:water on the TEM grid. Imaging was conducted at 120 keV with current densities below 70 pA/cm^2 to avoid beam damage to the organic−inorganic composite nanoparticles. The log-normal mean and standard deviation were determined using ImageJ software (freeware available through NIH) to provide the particle diameter for each particle in TEM photomicrographs and PeakFit (v.4.12; Jandel Scientific, San Rafael, CA) to fit the diameter data to a log-normal distribution by area. The mean log-normal particle diameter is 16 nm with a log-normal standard deviation equal to 0.23 for 99% of the distribution. A second peak centered at 63 nm comprising 1% by area with a log-normal standard deviation equal to 0.01 was also determined by the log-normal probability fit. This latter peak is real as seen in the particles in the TEM in Figure 1. The log-normal standard deviation of 0.23 gives a value of 9 nm for −1 standard deviation and 27 nm for +1 standard deviation from the mean value.

Attachment of PEGamine to Carboxylic Acid Functionalized CPNPs. The as-synthesized particles with carboxylate functional groups were surface passivated with polyethylene glycol (PEG) *via* a secondary functionalization scheme. A 4 mL aliquot of the carboxylate−CPNPs (5×10^{13} particles) was chemically conjugated with methoxypolyethylene glycol amine (mPEG-amine) through an ethyl-*N*-(3-dimethylaminopropyl)-*N*′-hydrochloride carbodiimide (EDAC) reaction.[85] The sample was first stirred at 550 rpm on a combination magnetic stir/hot plate set to 50 °C. In a dropwise manner, 1 mL of EDAC (1 mg/mL) and 1 mL of mPEG-amine (10 mg/mL), both in aqueous solutions of CO_2-free DI water (pH 7), were added to the sample under continuous stirring, amounting to a calculated 6-fold excess for monolayer surface coverage. The particles were reacted for 15 h at 50 °C to form amide linkages between the carboxylate surfaces and the mPEG-amine. The mixture was then filtered through a centrifuge filter (Microsep 100K Omega; Pall Life Science, East Hills, NY) at 1000*g* for 40 min (Marathon 22K Centrifuge; Fischer Scientific, Pittsburgh, PA) to remove any excess EDAC and unreacted mPEG-amine. TEM characterization of the retentate showed that the PEG-CPNPs remained well dispersed after the centrifugation wash.

Optical Characterization of ICG-CPNPs. For all optical measurements, samples were placed in a low-volume fluorescence cuvette (9F-SOG-10-GL14-S; Starna Cells, Inc., Atascadero, CA) and held by a modified cuvette holder. Absorption spectra were recorded on a PerkinElmer Lambda 950 UV−vis−NIR spectrophotometer (Perkin-Elmer, Waltham, MA). The dye-doped particle absorption at 785 nm was compared to a standard curve of absorption *versus* ICG concentration to identify the apparent encapsulate content, though not accounting for any optical matrix effects. Next, the release of the encapsulated fluorophore was induced with the addition of a 10:1 volume ratio of a 10^{-3} M solution of ethylenediaminetetraacetic acid (EDTA) to the particle suspension. EDTA is a chelating agent that sequesters the divalent Ca^{2+} ion from the nanostructure, dissolving the calcium phosphate particles. The 785 nm absorption value of the released ICG was compared to a second standard curve of ICG in an EDTA−salt solution, isotonic to the solvent environment after nanoparticle dissolution. This procedure gave the true fluorophore concentration encapsulated within the particles.

Fluorescence spectra were recorded using an in-house spectroscopy system in which emitted radiation was collected at 90° with a 10X microscope objective (N.A. 0.3) coupled into a fiber optic cable leading to the spectrometer (HR-2000-USB; Ocean Optics, Dunedin, FL). A high-power 785 nm diode laser (450 mW/cm^2) was used as the excitation source (RL785; Renishaw plc, Gloucestershire, UK). Solvent influence was recorded on both free ICG and doped nanoparticle suspensions of comparable fluorophore content. Aliquots of each were diluted 1:10 into the test solvent and kept in the dark. Measurements were conducted precisely 10 min after the sample introduction.

Quantum efficiency measurements were conducted following the comparative method of Williams *et al.*,[86] for which a reference sample with identical absorbance at the same excitation wavelength of the unknown analyte is assumed to absorb the same number photons as the latter. Hence, the ratio of the integrated fluorescence intensities of the test solution to the reference of known efficiency yields the ratio of the quantum efficiency values, provided they are recorded under identical conditions. Hexamethylindotricarbocyanine (HITC) was selected as the standard fluorophore due to its similar absorption at the excitation wavelength of ICG; its quantum yield is well documented at 0.28 in methanol.[74] Each measurement was conducted in duplicate on two separate occasions using freshly prepared stock solutions and a new set of standard data. This comparative quantum efficiency determination was developed for molecular systems and, as such, does not take into account scattering or attenuation influences characteristic of particulate suspensions. However, the measured values are presented as a conservative approximation of quantum efficiency for the encapsulated fluorophore, as we expect adjustments for the attenuated light that actually reaches the encapsulated molecules within the highly scattering particle geometry would show a larger fluorescent ratio and thus yield higher efficiency values than reported.

The decay of the fluorescence with time for ICG was generated by recording the fluorescent spectra of both the free dye solution and doped nanoparticle suspension of equivalent fluorophore concentration at 5 s intervals under continuous illumination of the 785 nm laser. A set of measurements for each sample was conducted both at full laser power (100 mW) and at a reduced 11.6 mW power using an absorptive neutral density filter of +1.0 optical density (NE10A; Thor Laboratories, Newton, NJ). A 120 μL volume of each analyte was used to ensure simultaneous illumination over the entire analyte volume. Free ICG samples were diluted from the same 10^{-3} M stock solution. Measurements were recorded in duplicate using fresh solutions for each run.

***In Vivo* Animal Studies.** Four-week-old female nude mice (approximate weight of 15 g) were purchased from Harlan (Indianapolis, IN). All animal manipulations were performed with sterile technique and were approved by the Pennsylvania State University Institutional Animal Care and Use Committee.

Human breast adenocarcinoma cells (MDA-MB-231; American type Culture Collection, Manassas, VA) were cultured in DMEM supplemented with 10% fetal bovine serum (FBS). Exponentially growing cells were removed from the plate by trypsin/EDTA detachment, resuspended in PBS, and injected subcutaneously into both the right and left flank of the nude mice at approximately 10^6 cells per mouse. Tumors were allowed to grow to ~5 mm in diameter before the imaging trial was commenced.

Four different samples were prepared: ICG-CPNPs, both carboxylate terminated and PEGylated, a carboxylate-terminated blank CPNP suspension, and a 10^{-4} M solution of free ICG in deionized H_2O (pH 7). The latter two controls were designed to roughly match the estimated concentration of CPNPs (10^{13} particles/mL) and ICG content (10^{-5} M) in the injected solutions, respectively.

Sample aliquots for systemic injection were prepared in a 1:10 volume dilution in PBS. A 200 μL volume of each sample aliquot was injected into the tail vein of four nude mice. Near-infrared transillumination images were recorded using an In-Vivo FX whole animal imaging station (Kodak; Rochester, NY). The animals were placed into the imaging chamber, and anesthesia was induced and maintained by inhalation of 5% IsoSol vapor (isoflurane; Vedco, St. Joseph, MO) in 100% oxygen.

Each mouse was positioned flat on its abdomen side-by-side for simultaneous imaging. A 3 min exposure was recorded under NIR excitation using a 755 and 830 nm bandpass excitation and emission filter set, respectively. Next, an X-ray image (1 s exposure) was recorded of the mice in the same position to be used as an underlying reference. The separate NIR fluorescence and X-ray images were then merged to illustrate signal distribution relative to anatomy. This anesthesia and imaging procedure was repeated for each time point over a period of 96 h. The NIR images were pseudocolored and merged with the underlying X-ray images using Kodak MI imaging software (v.4; Kodak, Rochester, NY). The imaging studies were conducted on 20 mice for a total of 5 separate study groups.

***Ex Situ* Tissue Imaging.** Fluorescence signal intensity as a function of tissue depth was imaged for both free and encapsulated ICG of matching absorbance (10^{-4} M bulk ICG content) using a basic Sony DSC-P200 point-and-shoot camera (F3.5, 7 s exposure). The camera was modified to record wavelengths in the NIR by replacing the stock internal ICG/AA optics (modified by LPD, LLC; Carlstadt, NJ). The 100 μL aliquots were held in a 25 mm section of Tygon tubing (1 mm inner diameter) and front-face illuminated with a 780 nm 15 mW low divergence laser diode (LDM-5; Laserex Tech, Unley, Australia) fixed at 20° to the image plane. The camera was fitted with two 850 nm bandpass filters (FB850-40; Thor Laboratories, Newton, NJ) and positioned 20 cm from the tissue surface to capture the images. Kodak MI imaging software (v.4; Kodak, Rochester, NY) was used to pseudocolor the NIR image files and remove background noise. Porcine muscle tissue was purchased from a local butcher.

Acknowledgment. This work was made possible through the generous support of the Materials Research Institute at University Park and the Pennsylvania State Milton S. Hershey Medical Center, Pennsylvania State University. Partial support was also provided by Keystone Nano, Inc.

REFERENCES AND NOTES

1. Bornhop, D. J.; Contag, C. H.; Licha, K.; Murphy, C. J. Advances in Contrast Agents, Reporters, and Detection. *J. Biomed. Opt.* **2001**, *6*, 106–110.
2. Morawski, A. M.; Lanza, G. A.; Wickline, S. A. Targeted Contrast Agents for Magnetic Resonance Imaging and Ultrasound. *Curr. Opin. Biotechnol.* **2005**, *16*, 89–92.
3. Loo, C.; Lowery, A.; Halas, N.; West, J.; Drezek, R. Immunotargeted Nanoshells for Integrated Cancer Imaging and Therapy. *Nano Lett.* **2005**, *5*, 709–711.
4. Lin, A. W. H.; Lewinski, N. A.; West, J. L.; Halas, N. J.; Drezek, R. A. Optically Tunable Nanoparticle Contrast Agents for Early Cancer Detection: Model-Based Analysis of Gold Nanoshells. *J. Biomed. Opt.* **2005**, 10, 0604035.
5. Rao, J.; Dragulescu-Andrasi, A.; Yao, H. Fluorescence Imaging *In Vivo*: Recent Advances. *Curr. Opin. Biotechnol.* **2007**, *18*, 17–25.

6. Weissleder, R. A Clearer Vision for *In Vivo* Imaging. *Nat. Biotechnol.* **2001**, *19*, 316–317.
7. Sevick-Muraca, E. M.; Houston, J. P.; Gurfinkel, M. Fluorescence-Enhanced, Near Infrared Diagnostic Imaging with Contrast Agents. *Curr. Opin. Chem. Biol.* **2002**, *6*, 642–650.
8. Malicka, J.; Gryczynski, I.; Geddes, C. D.; Lakowicz, J. R. Metal-Enhanced Emission From Indocyanine Green: A New Approach to *In Vivo* Imaging. *J. Biomed. Opt.* **2003**, *8*, 472–478.
9. Benson, R. C.; Kues, H. A. Fluorescence Properties of Indocyanine Green as Related to Angiography. *Phys. Med. Biol.* **1978**, *23*, 159–163.
10. Yu, J.; Yaseen, M. A.; Anvari, B.; Wong, M. S. Synthesis of Near-Infrared-Absorbing Nanoparticle-Assembled Capsules. *Chem. Mater.* **2007**, *19*, 1277–1284.
11. Landsman, M. L. J.; Kwant, G.; Mook, G. A.; Zijlstra, W. G. Light-Absorbing Properties, Stability, and Spectral Stabilization of Indocyanine Green. *J. Appl. Physiol.* **1976**, *40*, 575–583.
12. Taichamn, G. C.; Hendry, P. J.; Wilbert, J. K. The Use of Cardio-Green for Intraoperative Vizualization of the Coronary Circulation: Evaluation of Myocardial Toxicity. *Tex. Heart I. J.* **1987**, *14*, 133–138.
13. Schutt, F.; Fischer, J.; Kopitz, J.; Holz, F. G. Indocyanine Green Angiography in the Presence of Subretinal or Intraretinal Haemorrhages: Clinical and Experimental Investigations. *Clin. Exp. Ophthalmol.* **2002**, *30*, 110–114.
14. Motomura, K.; Inaji, H.; Komoike, Y.; Kasugai, I.; Noguchi, S.; Koyama, H. Sentinel Node Biopsy Guided by Indocyanine Green Dye in Breast Cancer Patients. *Jpn. J. Clin. Oncol.* **1999**, *29*, 604–607.
15. Ishihara, H.; Okawa, H.; Iwakawa, T.; Umegaki, N.; Tsubo, T.; Matsuki, A. Does Indocyanine Green Accurately Measure Plasma Volume Early After Cardiac Surgery. *Anesth. Analg.* **2002**, *94*, 781–786.
16. Ott, P. Hepatic Elimination of Indocyanine Green with Special Reference to Distribution Kinetics and the Influence of Plasma Protein Binding. *Pharmacol. Toxicol.* **1998**, *82*, 1–48.
17. Paumgartner, G.; Probst, P.; Kraines, R.; Leevy, C. M. Kinetics of Indocyanine Green Removal from the Blood. *Ann. N.Y. Acad. Sci.* **1970**, *170*, 134–147.
18. Caesar, J.; Shaldon, S.; Chiandussi, L.; Guevara, L.; Sherlock, S. The Use of Indocyanine Green in the Measurement of Hepatic Blood Flow and as a Test of Hepatic Function. *Clin. Sci.* **1961**, *21*, 43–57.
19. Frangioni, J. V. *In Vivo* Near-Infrared Fluorescence Imaging. *Curr. Opin. Chem. Biol.* **2003**, *7*, 626–634.
20. Olsen, T. W.; Lim, J. I.; Capone, A.; Myles, R. A.; Gilman, J. P. Anaphylactic Shock Following Indocyanine Green Angiography. *Arch. Ophthalmol.* **1996**, *114*, 97.
21. Philip, R.; Penzkofer, A.; Baumler, W.; Szeimies, R. M.; Abels, C. Absorption and Fluorescence Spectroscopic Investigation of Indocyanine Green. *J. Photochem. Photobiol. A* **1996**, *96*, 137–148.
22. Soper, S. A.; Mattingly, Q. L. Steady-State and Picosecond Laser Fluorescence Studies of Nonradiative Pathways in Tricarbocyanine Dyes: Implications to the Design of Near-IR Fluorochromes with High Fluorescence Efficiencies. *J. Am. Ceram. Soc.* **1994**, *116*, 3744–3752.
23. Lakowicz, J. R. *Principles of Fluorescence Spectroscopy*, 3rd ed.; Springer: Baltimore, MD, 2006.
24. Yan, J.; Estevez, C.; Smith, J.; Wang, K.; He, X.; Wang, L.; Tan, W. Dye-Doped Nanoparticles for Bioanalysis. *Nano Today* **2007**, *2*, 44–50.
25. Desmettre, T.; Devoisselle, J. M.; Mordon, S. Fluorescence Properties and Metabolic Features of Indocyanine Green (ICG) as Related to Angiography. *Surv. Ophthalmol.* **2000**, *45*, 15–27.
26. Simmons, R.; Shephard, R. J. Does Indocyanine Green Obey Beer's Law. *J. Appl. Physiol.* **1971**, *30*, 502–507.
27. Gathje, J.; Steuer, R. R.; Nicholes, K. R. K. Stability Studies on Indocyanine Green Dye. *J. Appl. Physiol.* **1970**, *29*, 181–185.
28. Holzer, W.; Mauerer, M.; Penzkofer, A.; Szeimies, R. M.; Abels, C.; Landthaler, M.; Baumler, W. Photostability and Thermal Stability of Indocyanine Green. *J. Photochem. Photobiol. B* **1998**, *47*, 155–164.
29. Mordon, S.; Devoisselle, J. M.; Soulie-Begu, S.; Desmettre, T. Indocyanine Green: Physicochemical Factors Affecting its Fluorescence *In Vivo*. *Microvasc. Res.* **1998**, *55*, 146–152.
30. Maarek, J. M. I.; Holschneider, D. P.; Harimoto, J. Fluorescence of Indocyanine Green in Blood: Intensity Dependence on Concentration and Stabilization with Sodium Polyaspartate. *J. Photochem. Photobiol. B* **2001**, *65*, 157–164.
31. Zhang, Y.; Wang, M. The Luminescent Properties and Photo-Decay of Sulfosalicylic Acid Doped ORMOSILs. *Mater. Lett.* **2000**, *42*, 86–91.
32. Saxena, V.; Sadoqi, M.; Shao, J. Degradation Kinetics of Indocyanine Green in Aqueous Solution. *J. Pharm. Sci.* **2003**, *92*, 2090–2097.
33. Muckle, T. J. Plasma Proteins Binding of Indocyanine Green. *Biochem. Med.* **1976**, *15*, 17–21.
34. Jin, S.; Ye, K. Nanoparticle-Mediated Drug Delivery and Gene Therapy. *Biotechnol. Prog.* **2006**, *23*, 32–41.
35. Sharma, P.; Brown, S.; Walter, G.; Santra, S.; Moudgil, B. Nanoparticles for Bioimaging. *Adv. Colloid Interface Sci.* **2006**, *123*, 471–485.
36. Devoisselle, J. M.; Soulie-Begu, S.; Mordon, S.; Desmettre, T.; Maillols, H. A Preliminary Study of the *In Vivo* Behaviour of an Emulsion Formulation of Indocyanine Green. *Laser Med. Sci.* **1998**, *13*, 279–282.
37. Zhao, X.; Bagwe, R. P.; Tan, W. Development of Organic-Dye-Doped Silica Nanoparticles in a Reverse Microemulsion. *Adv. Mater.* **2004**, *16*, 173–176.
38. Ow, H.; Larson, D. R.; Srivastava, M.; Baird, B. A.; Webb, W. W.; Wiesner, U. Bright and Stable Core-Shell Fluorescent Silica Nanoparticles. *Nano Lett.* **2005**, *5*, 113–117.
39. Zhou, X.; Zhou, J. Improving the Signal Sensitivity and Photostability of DNA Hybridizations on Microarrays by Using Dye-Doped Core-Shell Silica Nanoparticles. *Anal. Chem.* **2004**, *76*, 5302–5312.
40. Bele, M.; Siiman, O.; Matijevic, E. Preparation and Flow Cytometry of Uniform Silica-Fluorescent Dye Microspheres. *J. Colloid Interface Sci.* **2002**, *254*, 274–282.
41. Avnir, D.; Levy, D.; Reisfeld, R. The Nature of the Silica Cage as Reflected by Spectral Changes and Enhanced Photostability of Trapped Rhodamine 6G. *J. Phys. Chem.* **1984**, *88*, 5956–5959.
42. Burns, A.; Sengupta, P.; Zedayko, T.; Baird, B.; Wiesner, U. Core/Shell Fluorescent Silica Nanoparticles for Chemical Sensing: Towards Single-Particle Laboratories. *Small* **2006**, *6*, 723–726.
43. Soppimath, K. S.; Aminabhavi, T. M.; Kulkarni, A. R.; Rudzinski, W. E. Biodegradable Polymeric Nanoparticles as Drug Delivery Devices. *J. Controlled Release* **2001**, *70*, 1–20.
44. Saxena, V.; Sadoqi, M.; Shao, J. Indocyanine Green-Loaded Biodegradable Nanoparticles: Preparation, Physicochemical Characterization and *In Vitro* Release. *Int. J. Pharm.* **2004**, *278*, 293–301.
45. Yaseen, M. A.; Yu, J.; Wong, S. M.; Anvari, B. Laser-Induced Heating of Dextran-Coated Mesocapsules Containing Indocyanine Green. *Biotechnol. Prog.* **2007**, *23*, 1431–1440.
46. Gomes, A. J.; Lunardi, L. O.; Marchetti, J. M.; Lunardi, C. N.; Tedesco, A. C. Indocyanine Green Nanoparticles Useful for Photomedicine. *Photomed. Laser Surg.* **2006**, *24*, 514–521.
47. Saxena, V.; Sadoqi, M.; Shao, J. Enhanced Photo-Stability, Thermal-Stability and Aqueous-Stability of Indocyanine Green in Polymeric Nanoparticulate Systems. *J. Photochem. Photobiol. B* **2004**, *74*, 29–38.
48. Rodriguez, V. B.; Henry, S. M.; Hoffman, A. S.; Stayton, P. S.; Li, X.; Pun, S. H. Encapsulation and Stabilization of Indocyanine Green within Poly(Styrene-Alt-Maleic Anhydride) Block-Poly(Styrene) Micelles for Near-Infrared Imaging. *J. Biomed. Opt.* **2008**, *13*, 14025-1–14025-10.

49. Kim, G.; Huang, S.; Day, K. C.; O'Donnell, M.; Agayan, R. R.; Day, M. A.; Kopelman, R.; Ashkenazi, S. Indocyanine-Green-Embedded PEBBLEs as a Contrast Agent for Photoacoustic Imaging. *J. Biomed. Opt.* **2007**, 12, 044020.
50. Goldberg, M.; Langer, R.; Jia, X. Nanostructured Materials for Applications in Drug Delivery and Tissue Engineering. *J. Biomater. Sci., Polym. Ed.* **2007**, *18*, 241–268.
51. Gao, H.; Shi, W.; Freund, L. B. Mechanics of Receptor-Mediated Endocytosis. *Proc. Natl. Acad. Sci. U.S.A.* **2005**, *102*, 9469–9474.
52. Dorozhkin, S. V.; Epple, M. Biological and Medical Significance of Calcium Phosphates. *Angew. Chem., Int. Ed.* **2002**, *41*, 3130–3146.
53. Weber, J. N.; White, E. W.; Lebiedzik, J. New Porous Biomaterials Replication of Echinoderm Skeletal Microstructures. *Nature* **1971**, *233*, 337–339.
54. Dubok, V. A. Bioceramics—Yesterday, Today, Tomorrow. *Powder Metall. Met. Ceram.* **2000**, *39*, 381–394.
55. Chiroff, R. T.; White, R. A.; White, E. W.; Weber, J. N.; Roy, D. M. The Restoration of Articular Surfaces Overlying Porous Biomaterials. *J. Biomed. Mater. Res.* **1977**, *11*, 165–178.
56. He, Q.; Mitchell, A. R.; Johnson, S. L.; Wagner-Bartak, C.; Morcol, T.; Bell, S. J. D. Calcium Phosphate Nanoparticle Adjuvant. *Clin. Diagn. Lab. Immunol.* **2000**, *7*, 899–903.
57. Jeng, H. A.; Swanson, J. Toxicity of Metal Oxide Nanoparticles in Mammalian Cells. *J. Environ. Sci. Health A* **2006**, *41*, 2699–2711.
58. Derfus, A. M.; Chan, W. C. W.; Bhatia, S. N. Probing the Cytotoxicity of Semiconductor Quantum Dots. *Nano Lett.* **2004**, *4*, 11–18.
59. Colvin, V. L. The Potential Environmental Impact of Engineered Nanomaterials. *Nat. Biotechnol.* **2003**, *21*, 1166–1170.
60. Chang, E.; Thekkek, N.; Yu, W. W.; Colvin, V. L.; Drezek, R. Evaluation of Quantum Dot Cytotoxicity Based on Intracellular Uptake. *Small* **2006**, *2*, 1412–1417.
61. Lovrić, J.; Bazzi, H. S.; Cuie, Y.; Fortin, G. R. A.; Winnik, F. M.; Maysinger, D. Differences in Subcellular Distribution and Toxicity of Green and Red Emitting CdTe Quantum Dots. *J. Mol. Med.* **2005**, *83*, 377–385.
62. Hardman, R. A Toxicologic Review of Quantum Dots: Toxicity Depends on Physiochemical and Environmental Factos. *Environ. Health Persp.* **2006**, *114*, 165–172.
63. Oyane, A.; Kim, H.; Furuya, T.; Kobuko, T.; Miyazaki, T.; Nakamura, T. Preparation and Assessment of Revised Simulated Body Fluids. *J. Biomed. Mater. Res. A* **2002**, *65A*, 188–195.
64. Radin, S.; Campbell, J. T.; Ducheyne, P.; Cuckler, J. M. Calcium Phosphate Ceramic Coatings as Carriers of Vancomycin. *Biomaterials* **1997**, *18*, 777–782.
65. Bisht, S.; Bhakta, G.; Mitra, S.; Maitra, A. pDNA Loaded Calcium Phosphate Nanoparticles: Highly Efficient Non-Viral Vector for Gene Delivery. *Int. J. Pharm.* **2005**, *288*, 157–168.
66. Schmidt, H. T.; Gray, B. L.; Wingert, P. A.; Ostafin, A. Assembly of Aqueous-Cored Calcium Phosphate Nanoparticles for Drug Delivery. *Chem. Mater.* **2004**, *16*, 4942–4947.
67. Olton, D.; Li, J.; Wilson, M. E.; Rogers, T.; Close, T.; Close, J.; Huang, L.; Kumta, P. N.; Sfeir, C. Nanostructured Calcium Phosphate (NanoCaPs) for Non-Viral Gene Delivery: Influence of Synthesis Parameters on Transfection Efficiency. *Biomaterials* **2007**, *28*, 1267–1279.
68. Roy, I.; Mitra, S.; Maitra, A.; Mozumdar, S. Calcium Phosphate Nanoparticles as Novel Non-Viral Vectors for Targeted Gene Delivery. *Int. J. Pharm.* **2003**, *250*, 25–33.
69. Sokolova, V.; Prymak, O.; Meyer-Zaika, W.; Colfen, H.; Rehage, H.; Shukla, A.; Epple, M. Synthesis and Characterization of DNA-Functionalized Calcium Phosphate Nanoparticles. *Materalwiss. Werkstofftech* **2006**, *37*, 441–445.
70. Schmidt, H. T.; Ostafin, A. E. Liposome Directed Growth of Calcium Phosphate Nanoshells. *Adv. Mater.* **2002**, *14*, 532–535.
71. Adair, J. H.; Kumar, R.; Antolino, N.; Szepesi, C.; Kimel, R. A.; Rouse, S. M. Colloidal Lessons for Dispersion of Nanosize Particulate Suspensions. In *Proceedings of the World Academy of Ceramics*; Cesenatico, Italy, 2004.
72. Wang, J.; White, W. B.; Adair, J. H. Dispersion of SiO_2-Based Nanocomposites with High Performance Liquid Chromatography. *J. Phys. Chem. B* **2006**, *110*, 4679–4685.
73. Reindl, S.; Penzkofer, A.; Gong, S. H.; Landthaler, M.; Szeimies, R. M.; Abels, C.; Baumler, W. Quantum Yield of Triplet Formation for Indocyanine Green. *J. Photochem. Photobiol. A* **1997**, *105*, 65–68.
74. Duggan, J. X.; DiCesare, J.; Williams, J. F. Investigations on the Use of Laser Dyes as Quantum Counters for Obtaining Corrected Fluorescence Spectra in the Near Infrared. In *New Directions in Molecular Luminescence*; Eastwood, D., Ed. American Society for Testing and Materials: ASTM STP 1983; Vol. 822, pp 112−126.
75. Penzkofer, A.; Lu, Y. Absorption Behavior of Methanolic Rhodamine 6G Solutions at High-Concentration. *Chem. Phys.* **1986**, *107*, 175–184.
76. De Grand, A. M.; Frangioni, J. V. An Operational Near-Infrared Fluorescence Imaging System Prototype for Large Animal Surgery. *Technol. Cancer Res. T* **2003**, *2*, 553–562.
77. Saxena, V.; Sadoqi, M.; Shao, J. Polymeric Nanoparticulate Delivery System for Indocyanine Green: Biodistribution in Healthy Mice. *Int. J. Pharm.* **2006**, *308*, 200–204.
78. Kong, G.; Braun, R. D.; Dewhirst, M. W. Hyperthermia Enables Tumor-Specific Nanoparticle Delivery: Effect of Particle Size. *Cancer Res.* **2000**, *60*, 4440–4445.
79. Maeda, H. The Enhanced Permeability and Retention (EPR) Effect in Tumor Vasculature: The Key Role of Tumor-Selective Macromolecular Drug Targeting. *Adv. Enzyme Regul.* **2001**, *41*, 189–207.
80. Maeda, H.; Fang, J.; Inutsuka, T.; Kitamoto, Y. Vascular Permeability Enhancement in Solid Tumor: Various Factors, Mechanisms Involved and its Implications. *Int. Immunopharmocol.* **2003**, *3*, 319–328.
81. Dvorak, H. F.; Nagy, J. A.; Dvorak, J. T.; Dvorak, A. M. Identification and Characterization of the Blood Vessels of Solid Tumors that are Leaky to Circulating Macromolecules. *Am. J. Pathol.* **1988**, *133*, 95–109.
82. Ballou, B.; Lagerholm, B. C.; Ernst, L. A.; Bruchez, M. P.; Waggoner, A. S. Noninvasive Imaging of Quantum Dots in Mice. *Bioconjugate Chem.* **2004**, *15*, 79–86.
83. James, W. D.; Hirsch, L. R.; West, J. L.; O'Neal, P. D.; Payne, J. D. Application of INAA to the Build-Up and Clearance of Gold Nanoshells in Clinical Studies in Mice. *J. Radioanal. Nucl. Chem.* **2007**, *271*, 455–459.
84. Cheong, W. F.; Prahl, S. A.; Welch, A. J. A Review of the Optical Properties of Biological Tissues. *IEEE J. Quantum Elect.* **1990**, *26*, 2166–2185.
85. Sharma, R. K.; Das, S.; Maitra, A. Surface Modified Ormosil Nanoparticles. *J. Colloid Interface Sci.* **2004**, *277*, 342–346.
86. Williams, A. T. R.; Winfield, S. A.; Miller, J. N. Relative Fluorescence Quantum Yields Using a Computer-Controlled Luminescence Spectrometer. *Analyst* **1983**, *108*, 1067–1071.